# Supplementary Materials

## Key role of short-lived halogens on global atmospheric oxidation during historical periods

Adriana Bossolasco[1,2], Rafael P. Fernandez[3,4], Qinyi Li[5], Anoop S. Mahajan[6], Julian Villamayor[1], Javier A. Barrera[7], Dwayne E. Heard[8], Carlos A. Cuevas[1], Cyril Caram[9], Sophie Szopa[9], and Alfonso Saiz-Lopez[1*]

[1]Department of Atmospheric Chemistry and Climate, Institute of Physical Chemistry Blas Cabrera, CSIC, Madrid, Spain.

[2]Physics Institute of Northwest Argentina (INFINOA-CONICET-UNT) - Tucumán, Argentina.

[3]Institute for Interdisciplinary Science (ICB), National Research Council (CONICET), Mendoza, Argentina.

[4]School of Natural Sciences (FCEN), National University of Cuyo (UNCuyo), Mendoza, Argentina.

[5]Environment Research Institute, Shandong University, Qingdao, China.

[6]Indian Institute of Tropical Meteorology, Ministry of Earth Sciences, Pune, India.

[7]Research Institute for Physical Chemistry of Córdoba, National Scientific and Technical Research Council (INFIQC-CONICET), Córdoba, Argentina. 4b. Department of Physical Chemistry, School of Chemical Sciences. National University of Córdoba (UNC), Córdoba, Argentina

[8]School of Chemistry, University of Leeds, Leeds, LS2 9JT, UK.

[9]Laboratoire des Sciences du Climat et de l'Environnement, LSCE/IPSL, CEA-CNRS-UVSQ, Université Paris-Saclay, Gif-sur-Yvette, France

Corresponding author: Alfonso Saiz-Lopez (a.saiz@csic.es)

**Tables:**

**Table S1:** Burden at the troposphere, surface and boundary layer for each Xy (Cly, Bry and Iy) specie in both cases (*wSLH* and *noSLH*) at present (PD) and pre-industrial (PI) times. The table also shows the ratio of burden between X (X =Cl, Br, I)/ $X_y$ for the *wSLH* case in present-day (PD) and pre-industrial (PI) times, respectively. The absolute burden values for X and $X_y$ are expressed in Gg.

| **Burden (Gg)** | | | | | | | | |
|---|---|---|---|---|---|---|---|---|
| | | **Troposphere** | **Surface** | **Boundary Layer** | | **Troposphere** | **Surface** | **Boundary Layer** |
| PD *wSLH* | **$Cl_y$** | 302 | 6 | 96 | PD *noSLH* | 32 | 0.11 | 3 |
| | **$Br_y$** | 21 | 0.6 | 7 | | 0.9 | $3.5x10^{-3}$ | $9 x10^{-2}$ |
| | **$I_y$** | 16 | 0.8 | 6 | | $1.4x10^{-5}$ | $4x10^{-7}$ | $6x10^{-6}$ |
| PI w*SLH* | **$Cl_y$** | 200 | 3 | 59 | PI no*SLH* | 17 | 0.07 | 2 |
| | **$Br_y$** | 17 | 0.3 | 4.5 | | 0.5 | $2 x10^{-3}$ | $7x10^{-2}$ |
| | **$I_y$** | 13 | 0.5 | 4 | | $1.5x10^{-5}$ | $4 x10^{-7}$ | $7x10^{-6}$ |

| **Ratio $Cl/Cl_Y$** | | | |
|---|---|---|---|
| | **Troposphere** | **Surface** | **Boundary Layer** |
| PD *wSLH* | $6.2x10^{-6}$ | $2.2x10^{-6}$ | $1.6x10^{-6}$ |
| | | | |
| PI *wSLH* | $1.2x10^{-5}$ | $8.1x10^{-6}$ | $5x10^{-5}$ |
| | | | |
| **PD/PI** | **0.52** | **0.27** | **0.32** |
| **Relation $Br/Br_Y$** | | | |
| PD *wSLH* | 0.017 | $3.7x10^{-3}$ | $4.1x10^{-3}$ |
| | | | |
| PI *wSLH* | 0.028 | $7.6x10^{-3}$ | $7.7x10^{-3}$ |
| | | | |
| **PD/PI** | **0.62** | **0.5** | **0.52** |
| **Relation $I/I_Y$** | | | |
| PD *wSLH* | **$9.1x10^{-2}$** | **$3.5x10^{-2}$** | **$4.1x10^{-2}$** |
| | | | |
| PI *wSLH* | **$1.4x10^{-1}$** | **$8.1x10^{-2}$** | **$8x10^{-2}$** |
| | | | |
| **PD/PI** | **0.67** | **0.43** | **0.51** |

$Cl_Y = Cl + 2*Cl_2 + ClO + HCl + HOCl + ClONO_2 + ClNO_2 + OClO + BrCl + ICl + 2*Cl_2O_2$

$Br_Y = Br + 2*Br_2 + BrO + HBr + HOBr + BrONO_2 + BrNO_2 + BrCl + IBr$

$I_Y = I + 2*I_2 + IO + HI + HOI + IONO_2 + INO_2 + OIO + INO + IBr + ICl + 2*I_2O_2 + 2*I_2O_3 + 2*I_2O_4.$

**Table S2:** Burdens of OH, $NO_3$, $O_3$ and Cl (expressed in Mg) in the boundary layer (BL, 1000-850 hPa) in different regions (Land, Ocean and Global) for *wSLH* and *noSLH* simulations for present (PD) and pre-industrial (PI) periods and its respectively relative percentage of change (%Δ) in oxidant concentrations due to SLH. %Δ = ((OxwSLH - OxnoSLH) / OxnoSLH ) * 100%, Ox= OH, $NO_3$, $O_3$ and Cl.

| **PD** | | | | | | | | | | | | |
|---|---|---|---|---|---|---|---|---|---|---|---|---|
| | | **OH** | | | **$O_3$** | | | **$NO_3$** | | | **Cl** | |
| | *wSLH* | *noSLH* | **%Δ** | *wSLH* | *noSLH* | **%Δ** | *wSLH* | *noSLH* | **%Δ** | *wSLH* | *noSLH* | **%Δ** |
| **Global** | 24 | 21 | **-16** | $3.4x10^7$ | $4.6x10^7$ | **-26** | $1.7x10^3$ | $2.8x10^3$ | **-38** | 0.15 | $5.6x10^{-3}$ | **2632** |
| **Land** | 4.9 | 5.3 | **-7** | $7.2x10^6$ | $9.1x10^6$ | **-20** | $6.0x10^2$ | $8.4x10^2$ | **-22** | 0.03 | $7.8x10^{-4}$ | **3999** |
| **Ocean** | 13 | 16 | **-19** | $1.5x10^7$ | $2.2x10^7$ | **-29** | $6.2x10^2$ | $1.1x10^3$ | **-44** | 0.08 | $2.9x10^{-3}$ | **2679** |
| **PI** | | | | | | | | | | | | |
| | | **OH** | | | **$O_3$** | | | **$NO_3$** | | | **Cl** | |
| | *wSLH* | *noSLH* | **%Δ** | *wSLH* | *noSLH* | **%Δ** | *wSLH* | *noSLH* | **%Δ** | *wSLH* | *noSLH* | **%Δ** |
| **Global** | 21 | 28 | **-25** | $2.0x10^7$ | $3.0x10^7$ | **-32** | $3.0x10^2$ | $5.9x10^2$ | **-49** | 0.29 | $9.1x10^{-3}$ | **3114** |
| **Land** | 4.0 | 4.6 | **-13** | $4.0x10^6$ | $5.5x10^6$ | **-28** | $1.6x10^2$ | $2.6x10^2$ | **-38** | 0.06 | $1.2x10^{-3}$ | **4954** |
| **Ocean** | 12 | 1.7 | **-29** | $9.5x10^6$ | $1.4x10^7$ | **-34** | $5.9x10^1$ | $1.4x10^2$ | **-59** | 0.16 | $4.9x10^{-3}$ | **3068** |

**Section 1:**

**A. Contribution of the Cl mechanism to increases oxidant loss**

While MDSA represents a significant source of chlorine in the boundary layer, its impact on global tropospheric OH reduction is relatively modest. Compared to simulations including short-lived halogens (SLHs) but excluding MDSA Cl production, the inclusion of MDSA mechanism increases the total OH decrease by approximately 3% in the present day (PD) and 8% in the pre-industrial (PI) periods. This can be explained by the major role that iodine and bromine play in destroying tropospheric O3 (1–3) and therefore regulating the OH decreases. As shown in Barrera et al., 2023(1), the total $O_3$ destruction in the PI and PD due to iodine is: -11% and -9%, bromine: -8% and -4% and Chlorine: -5% and -4%, respectively, while the total $O_3$ destruction by SLH is reported to be 21.1% and 15.5% in PI and PD, which is consistent with our results without considering MDSA (-24% and -22% for PI and PD, respectively). Important to note that Barrera et al., 2023(1) did not consider anthropogenic SLH emissions which are included in this study.

Our results (Table S3) shows that the additional ozone reduction due to Cl from MDSA account by approximately 4% and 8% during the PD and PI periods, leading to the aforementioned ~3% and 8% additional OH reduction. Thus, as can be seen from the values in Table S3, while MDSA contributes to greater oxidant reductions, its contribution (in %) is small compared to the overall effect of SLH emissions.

**Table S3:** Burdens of OH, $NO_3$, $O_3$ and Cl (expressed in Mg) in the boundary layer (BL, 1000-850 hPa) for *wSLH, wSLH noMDSA* and *noSLH* simulations for present (PD) and pre-industrial (PI) periods and its respectively relative percentage of change (%Δ) in oxidant concentrations due to SLH. %Δ = ((OxwSLH - OxnoSLH) / OxnoSLH) * 100%, Ox= OH, $NO_3$, $O_3$ and Cl.

| **PD** | | | | | | | | | | |
|---|---|---|---|---|---|---|---|---|---|---|
| **OH** | | | | | | **$O_3$** | | | | |
| | *wSLH* | *wSLH*$^{noMDSA}$ | *noSLH* | %Δ MDSA - noHAL | %Δ noMDSA -noHAL | *wSLH* | *wSLH*$^{noMDSA}$ | *noSLH* | %Δ MDSA-noHAL | %Δ noMDSA -noHAL |
| **Global** | 24 | 26 | 29 | **-16** | **-13** | $3.4x10^7$ | $3.6x10^7$ | $4.6x10^7$ | **-26** | **-22** |
| **$NO_3$** | | | | | | **Cl** | | | | |
| **Global** | $1.7x10^3$ | $1.9x10^3$ | $2.8x10^3$ | **-38** | **-30** | 0.15 | 0.05 | $5.6x10^{-3}$ | **2632** | **792** |
| **PI** | | | | | | | | | | |
| **OH** | | | | | | **$O_3$** | | | | |
| | *wSLH* | *wSLH*$^{noMDSA}$ | *noSLH* | %Δ MDSA - noHAL | %Δ noMDSA -noHAL | *wSLH* | *wSLH*$^{noMDSA}$ | *noSLH* | %Δ MDSA-noHAL | %Δ noMDSA -noHAL |
| **Global** | 21 | 23 | 28 | **-25** | **-17** | $2.0x10^7$ | $2.3x10^7$ | $3.0x10^7$ | **-32** | **-24** |
| **$NO_3$** | | | | | | **Cl** | | | | |
| **Global** | $3.0x10^2$ | $4x10^2$ | $5.9x10^2$ | **-49** | **-33** | 0.29 | 0.05 | $9.1x10^{-3}$ | **3114** | **423** |

## B. Comparison of the simulated dust deposition to observation

The Mineral Dust Entrainment and Deposition (DEAD) scheme used in this study (4) is the default dust emission scheme used in the CESM1 model configuration (5). Figure S1 shows the correlation between in-situ dust deposition measurements reported in Albani et al., 2014(6) and the total (wet and dry) dust deposition from the model. The model overestimates dust deposition in some regions over the Atlantic Ocean, Europe, Asia and Africa, which indicates that chlorine production in these areas might be overestimated. However, as was shown in Table S3, chlorine represents a minor contribution to the global oxidant reduction and therefore is not expected to have a large impact in the results of this work. A comparison of different dust emission schemes that are implemented in CESM2 is shown in Leung et al., 2024(7). They show that the new implementations improve the overall representation of dust in Earth System Models. However, using the DEAD scheme in CESM2, a later version of the model used in this study, shows similar regions where the model overestimates the dust deposition.

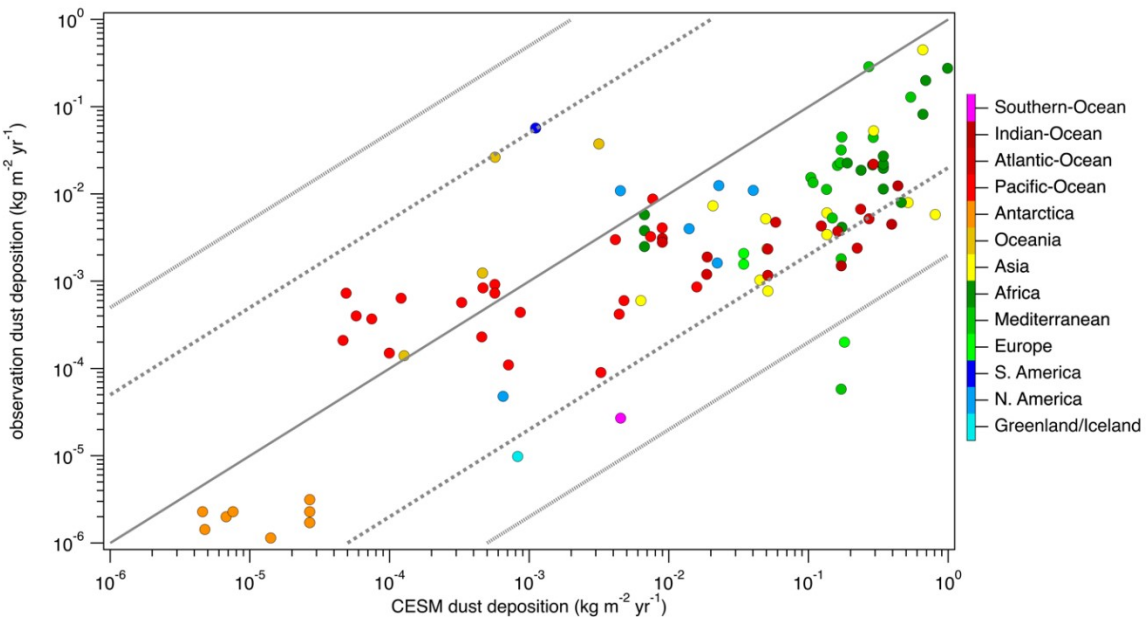

**Figure S1:** Observed dust deposition from ice cores, terrestrial deposits and marine sediments vs. total modeled dust deposition (wet+dry) in the same sites. Site locations are shown in color.

**Table S4**: **Comparison of global tropospheric OH (Tmol $yr^{-1}$) production rates between our simulation with and without Halogens and those reported in the literature.** Global annual mean tropospheric OH production for the primary (P) and secondary (S) sources of OH. G (gross OH formation) is the sum of $P + S$. The recycling probability (r) in % is calculated as $1-(P/P+S)$ *100%.

| Sources (Tmol $yr^{-1}$) | Lelieveld et al. 2002(8) | Lelieveld et al. 2016(9) | *noSLH* (PD) (this study) | *wSLH* (PD) (this study) |
|---|---|---|---|---|
| **Primary** | | | | |
| $O^1D + H_2O$ | 91.9 | 84.0 | 87 | 71 |
| **Secondary** | | | | |
| $NO + HO_2$ | | 76.6 | 59 | 56 |
| $O_3 + HO_2$ | | 34.4 | 22 | 17 |
| $H_2O_2 + h\nu$ | | 24.8 | 14 | 14 |
| OVOCs, ROOH +$h\nu$ | | 24.8 | 5.0 | 5.3 |
| HXO + $h\nu$ | | | - | 11 |
| Others | | | 0.2 | 0.2 |
| Total S | 96.2 | 167.2 | 100 | 103 |
| Total G (P + S) | 188.1 | 251.2 | 187 | 178 |
| **Recycling probability (%)** | 51 | 67 | 54 | 59 |

**Table S5: Global tropospheric $O_3$ and $CH_4$ burden (Tg) between our simulation and literature.**

| **Ozone Burden (Tg)** | [a] Sherwen et al. 2016(10) | [b] Caram et al. 2023(11) | | [c] Barerra et al. 2023(1) | | This Study | |
|---|---|---|---|---|---|---|---|
| | **PD** | **PI** | **PD** | **PI** | **PD** | **PI** | **PD** |
| ***noSLH*** | 416 | 281.9 | 317 | 233.4 | 328.8 | 232 | 326.4 |
| | | | | | | | |
| ***wSLH*** | 339 | 170.7 | 249.9 | 200.6 | 286.4 | 183 | 258.8 |
| **$CH_4$(Tg)** | [d]Li et al. 2022 | | | [e]Saiz-Lopez et al 2023 | | This Study | |
| | **PD** | | | **PI** | **PD** | **PI** | **PD** |
| ***noSLH*** | 4714.7 | | | 1755.6 | 4567.5 | 1510 | 3929 |
| | | | | | | | |
| ***wSLH*** | 5000.6 | | | 1997 | 4991 | 1715.5 | 4285 |

*PD: present day and PI: pre-industrial. Global tropospheric ozone burden (Tg) in the wSLH and noSLH case.*

[a]Sherwen, T. et al., 2016. have implemented atmospheric chemistry of halogenated species (Cl, Br, I) in the chemistry-transport model GEOS-Chem.

[b] Caram et al., 2023 have implemented atmospheric chemistry of halogenated species (Cl, Br, I) in the chemistry-climate model LMDZ-INCA.

[c] Barrera et al., 2023 use the Community Atmospheric Model with CAM-Chem, the scenario with full Halogens includes the complete representation of both sources and chemistry of natural Halogens.

[d] Li et al., 2022 conduct a set of long term (from the year 2000 to 2100) simulations using the CESM model and the Representative Concentration Pathway (RCP) scenarios, RCP6.0 and RCP8.5 to to evaluate the impact of SLHs.

[e]Saiz-Lopez et al., 2023 used CESM with CAM-Chem v 4.0 to quantify the overall impact of SLH on Earth's energy balance from pre-industrial times to the end of the twenty-first century.

**Figures:**

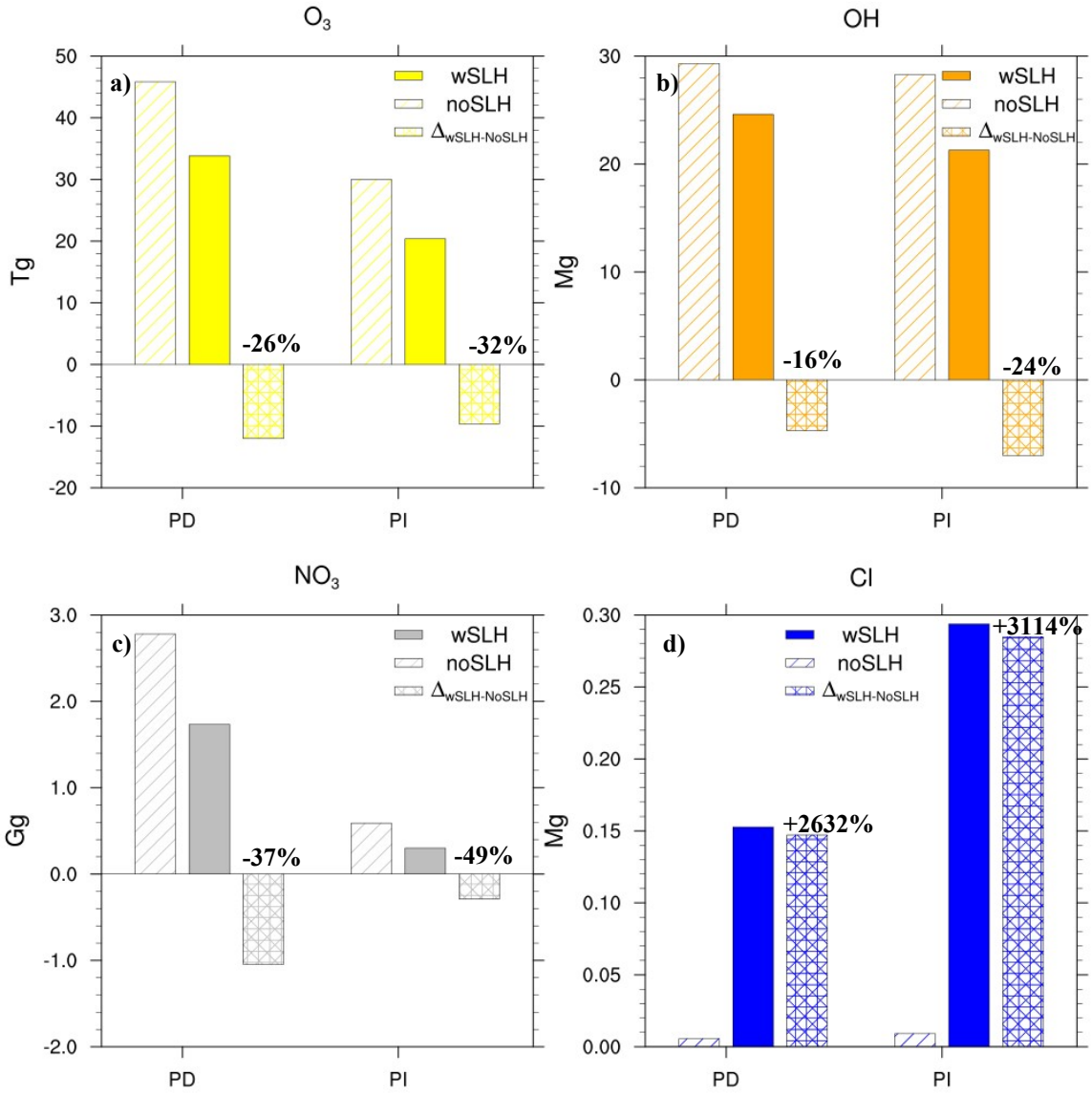


**Figure S2: Global integrated burden of main oxidants (OH, $O_3$, $NO_3$, and Cl) at the boundary layer (BL, 1000-850 hPa) and their relative changes due to the inclusion of SLH in the present-day (PD) and pre-industrial (PI) atmospheres**. Filled bars represent the *wSLH* case, hatched bars the *noSLH* case, and crosshatch bars the absolute differences between them. The relative percentage differences for PD and PI times are indicated above the bars in bold and are calculated as follow: % Δ Oxidant= $[Oxidant]_{wSLH}$- $[Oxidant]_{noSLH}$ / $[Oxidant]_{noSLH}$ **100%.* a) changes for $O_3$ (Tg), b) changes for OH (Mg), c) changes for $NO_3$ (Gg) and d) changes for Cl (Mg).

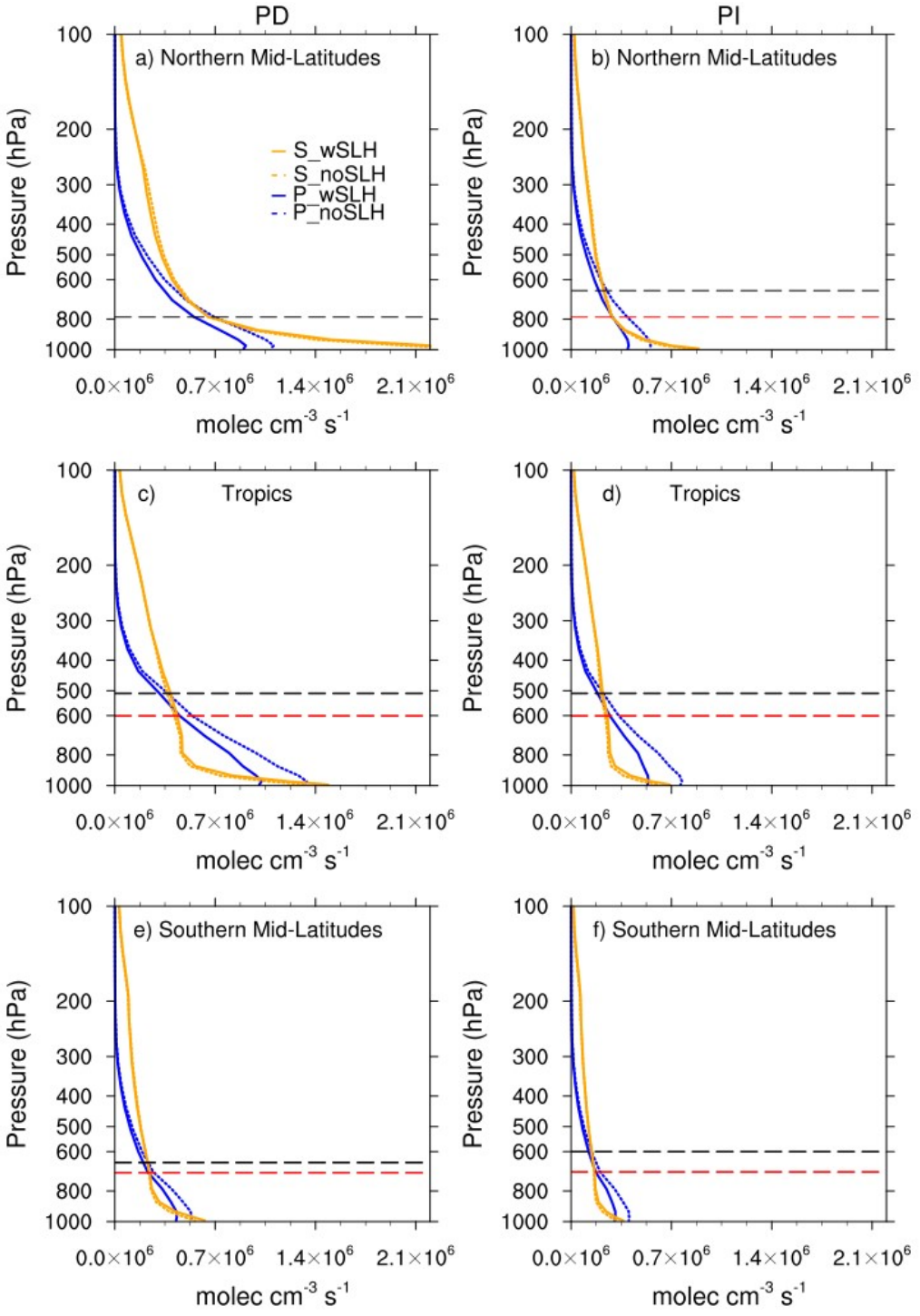


**Figure S3: Vertical profiles of primary (*P)* and secondary (*S)* OH production (molecules cm$^{-3}$ s$^{-1}$) for *wSLH* and *noSLH* cases for present (PD) and pre-industrial (PI) times in different latitudinal regions.** Vertical profiles of the primary (blue) and secondary (orange) sources OH production for *wSLH* (solid lines) and *noSLH* (dashed lines) cases in the PD average at a) Northern mid-latitudes (20º-50º N), c) Tropics (20ºS-20ºN) e) Southern mid-latitudes (20º-50º S). b), d) and f) similar to a), c) and e)

but for PI. The dashed horizontal lines denote the altitude pressure where *P* and *S* are equal (black: *noSLH* case, red: *wSLH* case).

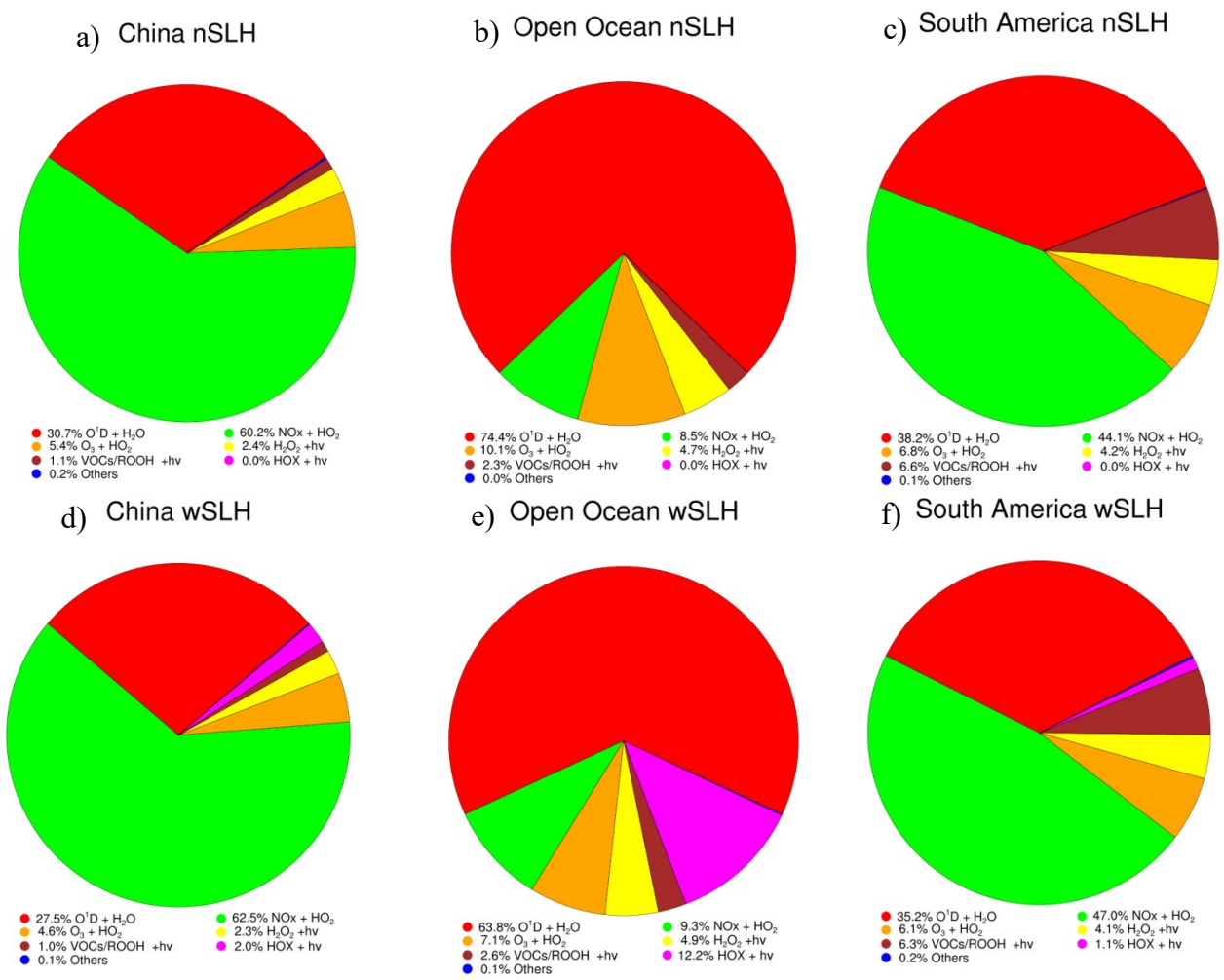


**Figure S4:** Changes in the BL OH production from the different reaction pathways (expressed in %) due to SLH at PD, for three selected regions: Polluted Regions: China (20-40 ºN, 100-125 ºE); Semi-Polluted Regions: South America (10-30 ºS, 70-40º W), Clean Regions: Open Ocean (0- 30ºN, 180-120 ºW).

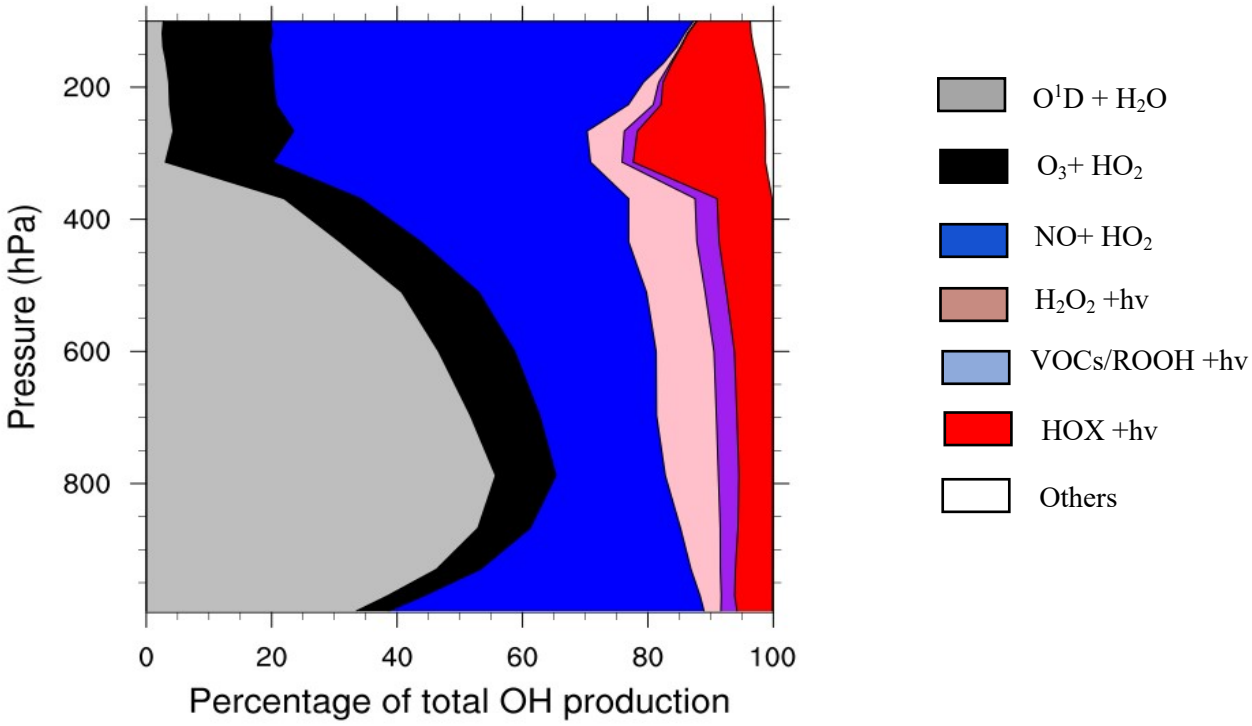


**Figure S5**: Global averaged vertical profile of the relative contribution of different OH production sources (in %) for the present-day (PD) with short-lived halogens (*wSLH*). The figure shows the percentage contribution of each source to the total OH production at different altitudes.

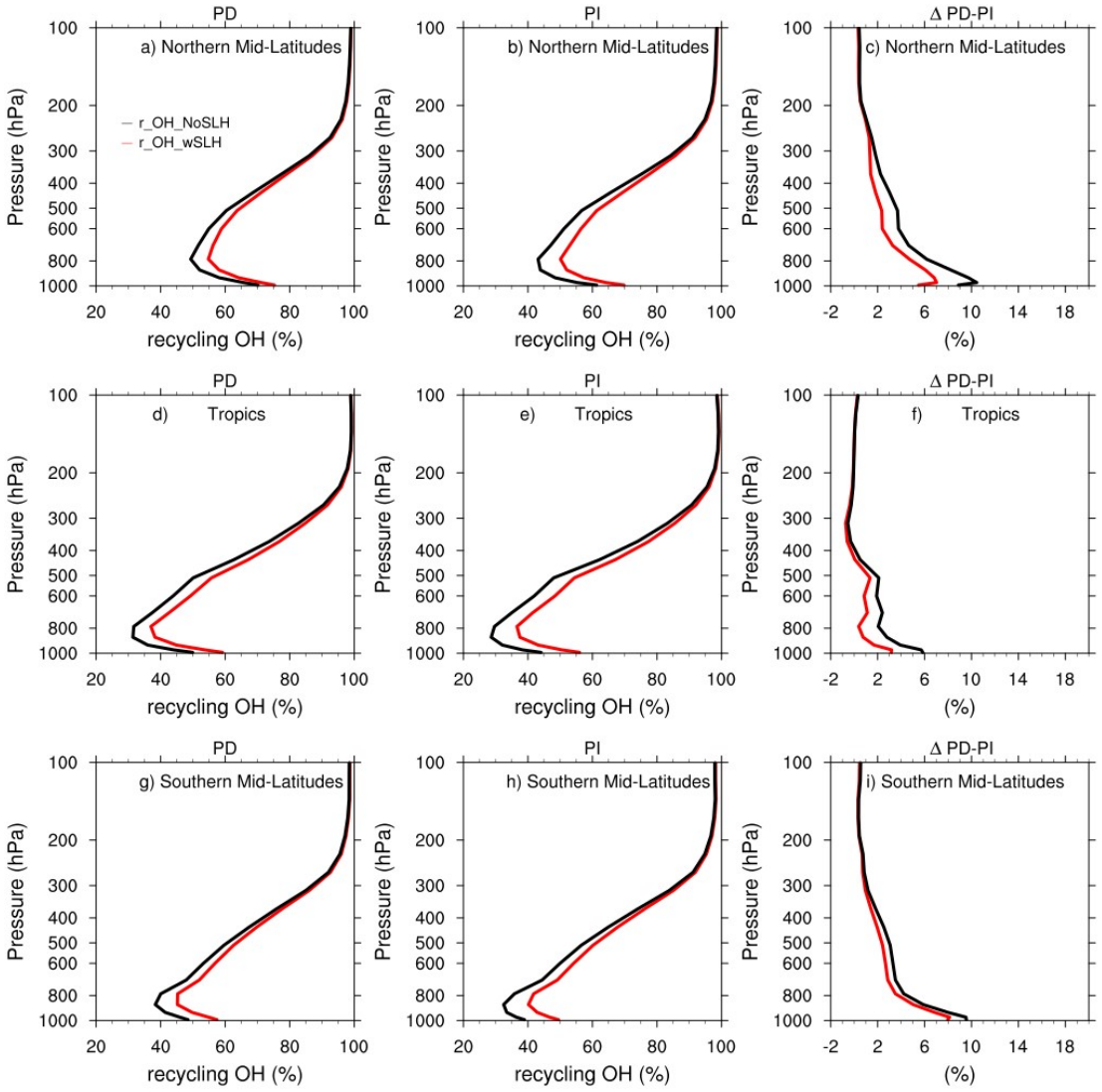


**Figure S6: Vertical profiles of recycling probability (r, %) for *wSLH* and *noSLH* simulations during present (PD) and pre-industrial (PI) periods at different latitudinal ranges.** Vertical profile for *wSLH* (red) and *noSLH* (black) cases in PD at a) Northern mid-latitudes (20º-50º N), d) Tropics (20ºS-20ºN) g) Southern mid-latitudes (20º-50º S). b), e) and h) similar to a), d) and g) but for PI. The right panels c), f), and i) show the changes in $r$ ($r_{PD}$- $r_{PI}$) for *wSLH* (red lines) and *noSLH* (black lines) in the corresponding regions.

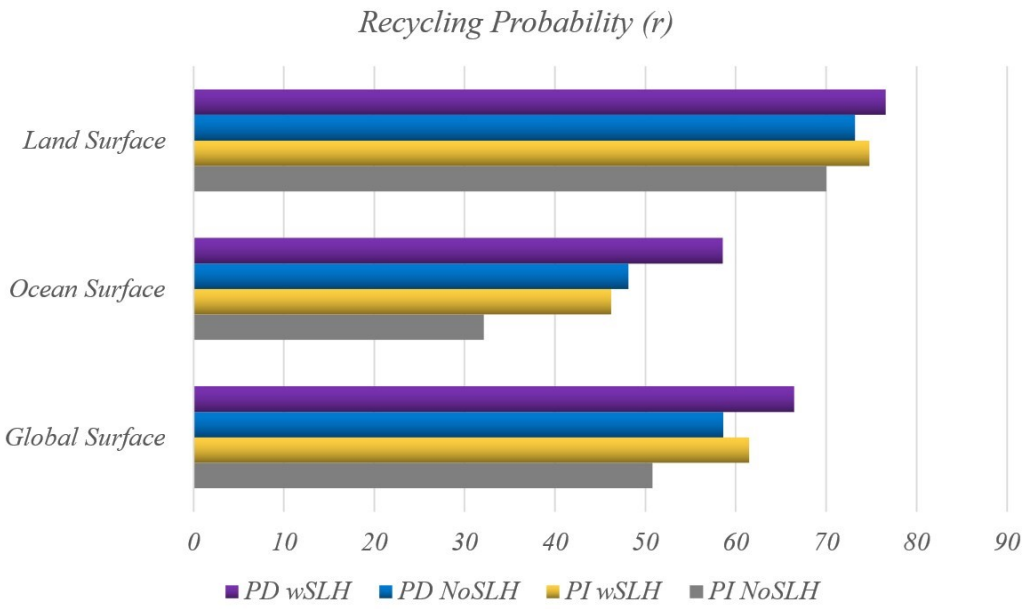


**Figure S7:** Global average values for the recycling probability (*r*) at the surface, ocean and land under different scenarios: present-day with SLH (PD wSLH), present-day without SLH (PD noSLH), pre-industrial with SLH (PI wSLH), and pre-industrial without SLH (PI noSLH). The increase in *r* due to SLH is generally larger over ocean surfaces compared to land surfaces.

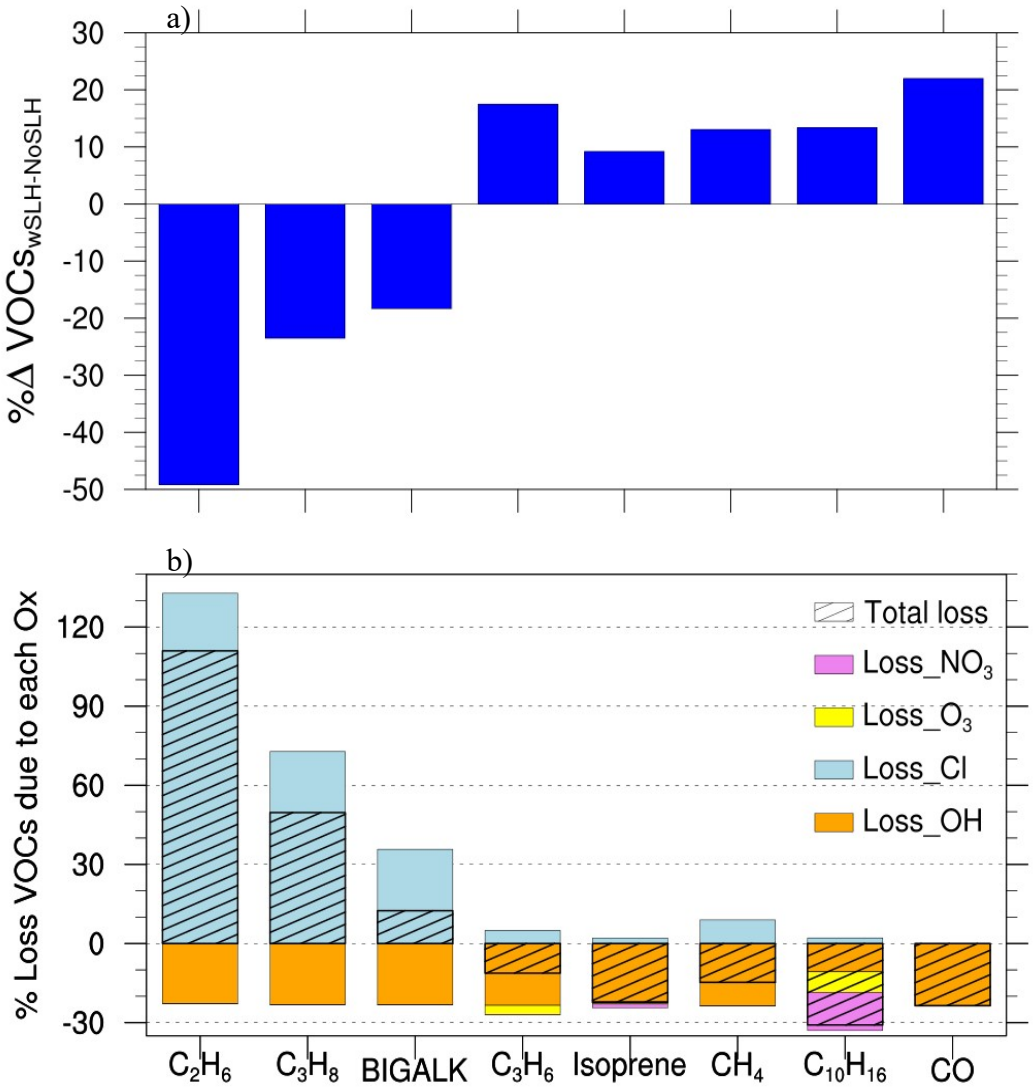


**Figure S8: Percentage of changes in the concentration of some principal VOCs due to the inclusion of *SLH* for pre-industrial (PI) times and the percentage contribution of each oxidant to VOC loss at the boundary layer (1000-850 hPa).** a) percentage changes in VOC concentrations due to SLH. b) the stacked bar chart shows the percentage contribution of each oxidant (OH, Cl, $O_3$ and $NO_3$) due to SLH to the total loss of VOCs. The calculation are based on the rate constants for the reaction of each VOC with the different oxidants and its relative change due to SLH, and was calculate as follow:

$$\Delta\ \%\ \text{loss VOCs Tot}_{\text{wSLH - noSLH}} = \frac{((k_{OH} * [OH] + k_{cl} * [Cl] + k_{O3} * [O_3] + k_{NO3} * [NO_3])_{wSLH} - (k_{OH} * [OH] + k_{cl} * [C}{(k_{OH} * [OH] + k_{cl} * [Cl] + k_{O3} * [O_3] + k_{NO3} * [NO_3}$$

*x 100*

$$\% \text{ contribution of loss by OH} = \frac{k_{OH} * [OH]_{wSLH} - k_{OH} * [OH]_{noSLH}}{(k_{OH} * [OH] + k_{cl} * [Cl] + k_{O3} * [O_3] + k_{NO3} * [NO_3])_{noSLH}} \times 100$$

$$\% \text{ contribution of loss by Cl} = \frac{k_{Cl} * [Cl]_{wSLH} - k_{Cl} * [Cl]_{noSLH}}{(k_{OH} * [OH] + k_{cl} * [Cl] + k_{O3} * [O_3] + k_{NO3} * [NO_3])_{noSLH}} \times 100$$

$$\% \text{ contribution of loss by } O_3 = \frac{k_{O3} * [O_3]_{wSLH} - k_{O3} * [O_3]_{noSLH}}{(k_{OH} * [OH] + k_{cl} * [Cl] + k_{O3} * [O_3] + k_{NO3} * [NO_3])_{noSLH}} \times 100$$

$$\% \text{ contribution of loss by } NO_3 = \frac{k_{NO3} * [NO_3]_{wSLH} - k_{NO3} * [NO_3]_{noSLH}}{(k_{OH} * [OH] + k_{cl} * [Cl] + k_{O3} * [O_3] + k_{NO3} * [NO_3])_{noSLH}} \times 100$$

where $k_{OH}$ is the rate constant for the loss of VOCs with OH and $k_{Cl}$ is the rate constant for the loss of VOCs with Cl, in the case of Isoprene, $C_3H_6$ and $C_{10}H_{16}$ we have also taken into account the loss due to $O_3$ and $NO_3$.

## References


1. Barrera JA, Kinnison DE, Fernandez RP, Lamarque JF, Cuevas CA, Tilmes S, et al. Comparing the Effect of Anthropogenically Amplified Halogen Natural Emissions on Tropospheric Ozone Chemistry Between Pre-Industrial and Present-Day. Journal of Geophysical Research: Atmospheres. 2023;128(14):e2022JD038283. Available from: https://agupubs.onlinelibrary.wiley.com/doi/abs/10.1029/2022JD038283

2. Badia A, Iglesias-Suarez F, Fernandez RP, Cuevas CA, Kinnison DE, Lamarque JF, et al. The Role of Natural Halogens in Global Tropospheric Ozone Chemistry and Budget Under Different 21st Century Climate Scenarios. Journal of Geophysical Research: Atmospheres. 2021;126(20):e2021JD034859. Available from: https://agupubs.onlinelibrary.wiley.com/doi/abs/10.1029/2021JD034859

3. Li Q, Fernandez RP, Hossaini R, Iglesias-Suarez F, Cuevas CA, Apel EC, et al. Reactive halogens increase the global methane lifetime and radiative forcing in the 21st century. Nat Commun. 2022;13(1):2768. Available from: https://doi.org/10.1038/s41467-022-30456-8

4. Zender CS, Bian H, Newman D. Mineral Dust Entrainment and Deposition (DEAD) model: Description and 1990s dust climatology. Journal of Geophysical Research: Atmospheres. 2003;108(D14). Available from: https://agupubs.onlinelibrary.wiley.com/doi/abs/10.1029/2002JD002775

5. Tilmes S, Lamarque JF, Emmons LK, Kinnison DE, Marsh D, Garcia RR, et al. Representation of the Community Earth System Model (CESM1) CAM4-chem within the Chemistry-Climate Model Initiative (CCMI). Geosci Model Dev. 2016;9(5):1853–90. Available from: https://gmd.copernicus.org/articles/9/1853/2016/

6. Albani S, Mahowald NM, Perry AT, Scanza RA, Zender CS, Heavens NG, et al. Improved dust representation in the Community Atmosphere Model. J Adv Model Earth Syst. 2014;6(3):541–70. Available from: https://agupubs.onlinelibrary.wiley.com/doi/abs/10.1002/2013MS000279

7. Leung DM, Kok JF, Li L, Mahowald NM, Lawrence DM, Tilmes S, et al. A new process-based and scale-aware desert dust emission scheme for global climate models – Part II: Evaluation in the Community Earth System Model version 2 (CESM2). Atmos Chem Phys. 2024;24(4):2287–318. Available from: https://acp.copernicus.org/articles/24/2287/2024/

8. Lelieveld J, Peters W, Dentener FJ, Krol MC. Stability of tropospheric hydroxyl chemistry. Journal of Geophysical Research: Atmospheres. 2002;107(D23):ACH 17-1-ACH 17-11. Available from: https://agupubs.onlinelibrary.wiley.com/doi/abs/10.1029/2002JD002272

9. Lelieveld J, Gromov S, Pozzer A, Taraborrelli D. Global tropospheric hydroxyl distribution, budget and reactivity. Atmos Chem Phys. 2016;16(19):12477–93. Available from: https://acp.copernicus.org/articles/16/12477/2016/

10. Sherwen T, Schmidt JA, Evans MJ, Carpenter LJ, Großmann K, Eastham SD, et al. Global impacts of tropospheric halogens (Cl, Br, I) on oxidants and composition in GEOS-Chem. Atmos Chem Phys. 2016;16(18):12239–71. Available from: https://acp.copernicus.org/articles/16/12239/2016/

11. Caram C, Szopa S, Cozic A, Bekki S, Cuevas CA, Saiz-Lopez A. Sensitivity of tropospheric ozone to halogen chemistry in the chemistry–climate model LMDZ-INCA vNMHC. Geosci Model Dev. 2023;16(14):4041–62. Available from: https://gmd.copernicus.org/articles/16/4041/2023/